

Isotopically heavy Ti in kimberlites explained by assimilation of metasomatised lithospheric mantle

Journal Article

Author(s):

Anguelova, Merislava; [Giuliani, Andrea](#) ; [Fehr, Manuela](#) ; [Schönbächler, Maria](#) 

Publication date:

2025

Permanent link:

<https://doi.org/https://doi.org/10.3929/ethz-c-000790717>

Rights / license:

[Creative Commons Attribution 4.0 International](#)

Originally published in:

Geochimica et Cosmochimica Acta, <https://doi.org/10.1016/j.gca.2025.12.005>

Funding acknowledgement:

- Tracking planet formation, differentiation and the moon-forming giant impact: an integrated approach using non-traditional stable isotopes ()
- Building Planets and Understanding Nucleosynthesis: Constraints from High-precision Isotope Analyses of Meteorites ()

Journal Pre-proofs

Isotopically heavy Ti in kimberlites explained by assimilation of metasomatised lithospheric mantle

Merislava Anguelova, Andrea Giuliani, Manuela A. Fehr, Maria Schönbächler

PII: S0016-7037(25)00676-3
DOI: <https://doi.org/10.1016/j.gca.2025.12.005>
Reference: GCA 14131

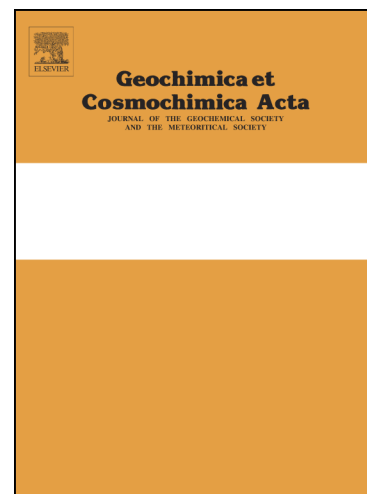
To appear in: *Geochimica et Cosmochimica Acta*

Received Date: 22 March 2025
Accepted Date: 2 December 2025

Please cite this article as: Anguelova, M., Giuliani, A., Fehr, M.A., Schönbächler, M., Isotopically heavy Ti in kimberlites explained by assimilation of metasomatised lithospheric mantle, *Geochimica et Cosmochimica Acta* (2025), doi: <https://doi.org/10.1016/j.gca.2025.12.005>

This is a PDF of an article that has undergone enhancements after acceptance, such as the addition of a cover page and metadata, and formatting for readability. This version will undergo additional copyediting, typesetting and review before it is published in its final form. As such, this version is no longer the Accepted Manuscript, but it is not yet the definitive Version of Record; we are providing this early version to give early visibility of the article. Please note that Elsevier's sharing policy for the Published Journal Article applies to this version, see: <https://www.elsevier.com/about/policies-and-standards/sharing#4-published-journal-article>. Please also note that, during the production process, errors may be discovered which could affect the content, and all legal disclaimers that apply to the journal pertain.

© 2025 The Author(s). Published by Elsevier Ltd.



Isotopically heavy Ti in kimberlites explained by assimilation of metasomatised lithospheric mantleMerislava Anguelova¹, Andrea Giuliani^{1, 2}, Manuela A. Fehr¹, Maria Schönbacher^{1*}¹ Institute of Geochemistry and Petrology, ETH Zürich, Switzerland² Earth and Planets Laboratory, Carnegie Institution for Science, Washington DC, United States

* Corresponding author: E-mail: mariasc@ethz.ch; Institute of Geochemistry and Petrology, ETH Zürich, Clausiusstrasse 25, 8092 Zürich, Switzerland; phone: +41 44 632 37 92

Abstract

Kimberlites represent some of the Earth's deepest sourced mantle melts, but the origin of their variable geochemical signatures is debated, including contributions by source variations and lithospheric interaction during ascent. To evaluate this further, the Ti isotope compositions of selected kimberlites ($n = 24$) from major cratons worldwide with emplacement ages from 1.15 Ga to the Holocene are reported. The kimberlites display variable Ti isotope compositions ranging from $+0.007 \pm 0.027 \text{ ‰}$ to $+0.173 \pm 0.027 \text{ ‰}$ for $\delta^{49}\text{Ti}$ (deviation of $^{49}\text{Ti}/^{47}\text{Ti}$ from the OL-Ti standard). The observed $\delta^{49}\text{Ti}$ variation of $\sim 0.17 \text{ ‰}$ is notably larger compared to typical mantle-derived primitive magmas (i.e. basalts and komatiites). Significant inter-province $\delta^{49}\text{Ti}$ variations are in contrast with negligible variations within each locality. Notably, primitive and highly differentiated kimberlites within the same kimberlite field display uniform Ti isotope compositions. These results contrast with the Ti isotope differentiation trends observed for silicate magmas, corroborating late-stage crystallisation of major Ti-carriers (i.e. spinel, perovskite, mica) in kimberlites, and may further indicate limited crystal-melt Ti isotope fractionation in carbonated silicate magmas. Heavy Ti isotope compositions observed in some kimberlites cannot be explained by the limited isotopic fractionation predicted between carbonated melts and peridotitic sources during partial melting, or by mixing of ambient mantle with subducted material, including terrigenous sediments with elevated $\delta^{49}\text{Ti}$. Instead, isotopically heavy Ti appears to occur in kimberlites featuring elevated concentrations of mica and low Mg/Fe in olivine, both considered a hallmark of extensive interaction of primary kimberlite melts with strongly metasomatised, Fe-Ti-rich lithospheric mantle. These observations underscore a dominant role of the lithospheric mantle in shaping the anomalously heavy Ti isotope compositions of kimberlites.

1. Introduction

Kimberlites are volatile-rich magmas formed by low-degree partial melting of the mantle at depths exceeding 150 km (e.g. Giuliani et al., 2023; Stamm and Schmidt, 2017). During their rapid ascent to the Earth's surface, they entrain xenoliths such as lower crustal fragments, mantle peridotites, and diamonds, providing direct insights into the subcontinental lithosphere and deeper mantle. Kimberlites preferentially occur within cratons worldwide and have been emplaced from the late Archaean to the Holocene (e.g. Tappe et al., 2018; Kjarsgaard et al., 2022). The nature of the source region, triggers of partial melting and parental melt composition of kimberlites are unresolved questions (Giuliani et al., 2023). It has been recently suggested that kimberlite melts sample an ancient mantle reservoir, which might have remained partially isolated for more than 2.5 billion years (Woodhead et al., 2019). Strontium, Nd and Hf isotope compositions and the spatial association of Phanerozoic kimberlites with seismic anomalies above the core-mantle boundary indicate that some kimberlites share a common deep-mantle source with ocean island basalts (OIBs, Giuliani et al., 2021; Pearson et al., 2019; Torsvik et al., 2010). Tungsten isotope studies on kimberlite rocks (Nakanishi et al., 2021; Tappe et al., 2020a), however, reached diverging conclusions regarding the source of kimberlite melts and the involvement of ancient material from as deep as the core-mantle boundary.

The mantle source reservoir of kimberlites younger than ~250 Ma was largely affected by recycling of subducted crustal material, as indicated by Sr, Nd, Hf and C isotope compositions of Mesozoic and Cenozoic kimberlites (Giuliani et al., 2022, 2025; Woodhead et al., 2019). Other studies (e.g. Dalton et al., 2022; Tappe et al., 2020b), however, showed that subducted material was already important in the genesis of some Precambrian kimberlites. In addition, kimberlites are well known to extensively interact with variously metasomatised lithospheric mantle wall rocks during ascent (e.g. Hunter and Taylor, 1982; Mitchell, 2008; Soltys et al., 2016; Giuliani et al., 2023). This process has been shown to affect the Mg-Fe systematics of kimberlites and related lamproite rocks (Dalton et al., 2020; Giuliani et al., 2020; Sarkar et al., 2021, 2022; Tovey et al., 2021), but may also influence the concentration of moderately incompatible elements such as Ti (Howarth et al., 2022) and, at least locally, strongly incompatible elements including Sr-Nd-Hf isotope systematics (Fitzpayne et al., 2023). It is therefore not always clear how to disentangle the roles of source heterogeneities and lithospheric-mantle interaction in the composition of kimberlites.

Titanium isotopes have emerged as a valuable tool for tracing igneous processes and mantle source features (Aarons et al., 2020; Anguelova et al., 2022; Deng et al., 2018, 2019, 2023; Greber et al., 2017a; Klaver et al., 2024; Kommescher et al., 2023; Millet et al., 2016) and have therefore the potential to shed light on some aspects of kimberlite petrogenesis. Komatiites and primitive basalts display limited Ti-isotope variation, with $\delta^{49}\text{Ti}$ (deviation of $^{49}\text{Ti}/^{47}\text{Ti}$ from the OL-Ti standard) values of ca. $+0.02 \pm 0.05$

‰, 2SD (e.g. Deng et al., 2018, 2023; Greber et al., 2017b; Millet and Dauphas, 2014; Millet et al., 2016; Zhao et al., 2020, 2024). Silica-rich magmas are enriched in isotopically heavy Ti due to significant Ti isotope fractionation during magmatic differentiation, driven by changes in Ti-coordination during Fe-Ti-oxide formation (e.g. Deng et al., 2019; Millet et al., 2016; Johnson et al., 2019; Hoare et al., 2020, 2022). In contrast, primitive (undifferentiated) ultrapotassic rocks, derived from metasomatised lithospheric mantle modified by subducted continental material, display Ti isotope compositions up to ~0.3 ‰ heavier than basalts, suggesting Ti isotopes may trace crust-mantle interaction (Anguelova et al., 2022). The heavy Ti isotope compositions were interpreted to reflect the signature of the subducted crustal components, possibly accompanied by Ti isotope fractionation during mobilisation from the slab in the presence of residual rutile (Anguelova et al., 2022). Similarly, Klaver et al. (2024) argued that high $\delta^{49}\text{Ti}$ values in primitive arc lavas result from Ti isotope fractionation during melting of the subducted slab and Spencer et al. (2024) attributed isotopically heavy Ti in sanukitoids and appinites to a metasomatised lithospheric mantle. Titanium isotopes therefore offer a new tool to explore potential geochemical variations in kimberlites, which might stem from either time-dependent source variability in response to recycling of crustal material, and/or interaction with metasomatised lithosphere during ascent. To address this issue, we present a comprehensive set of Ti isotope data for fresh, hypabyssal (i.e. subvolcanic) kimberlite rocks from different localities worldwide. The sample set comprises on-craton Proterozoic and Phanerozoic kimberlites with emplacement ages from ~1.15 Ga to the Holocene, including kimberlites that show various degrees of geochemical enrichment based on variable mica and hence K contents and Sr-Nd-Hf isotope systematics.

2. Samples

Representative kimberlites ($n = 24$) from 15 kimberlite fields worldwide (Fig. 1) were selected for Ti isotope analysis. The samples comprise predominantly fresh, calcite serpentine and/or monticellite kimberlites as well as mica-rich varieties (Fig. 2) and cover a wide age range of >1 billion years. To assess the extent to which kimberlite melt differentiation may fractionate Ti isotopes, evolved kimberlites with abundant carbonates and/or oxide minerals were also included in the sample set. A summary of the main petrographic features, age and geochemical information is presented in Table 1. Further details are provided in the Supplementary Material. The majority of the selected kimberlites were previously characterised for petrology, major- and trace element and radiogenic isotope geochemistry, with whole-rock data included in Table S1. We additionally measured 4 samples of olivine lamproite from South Africa ($n = 2$), United States (1) and India (1), the results of which are reported in Table S2.

3. Analytical methods

Sample chips free of xenoliths and megacrysts were powdered using either an agate disc mill or mortar. Sample digestion followed the procedure of Schönbacher et al. (2004). Approximately 100 mg of rock powder were dissolved in a 1:3 mixture of 23.5 M HF and 14 M HNO₃ in Parr® acid digestion bombs at 170°C for 4.5 days. Following evaporation, samples were re-dissolved in 6 M HCl and refluxed overnight to decompose precipitated fluorides. The resulting solutions did not contain any optically visible residue.

Chemical purification of Ti followed the protocol outlined in Williams et al. (2021) and Anguelova et al. (2024). Briefly, sample aliquots containing 20 µg Ti were mixed 1:1 with a ⁴⁷Ti-⁴⁹Ti double-spike. Spiked aliquots were refluxed overnight, dried down and re-dissolved in 6 M HCl twice to reach sample-spike homogenisation. Titanium was separated from the matrix via a three-step ion-exchange chromatographic procedure using Bio-Rad AG1-X8 anion exchange resin (100–200 and 200–400 mesh, chloride form). Total procedural blanks ranged between 1.0–1.5 ng Ti and were insignificant.

Titanium isotope analyses were performed using a Thermo Scientific Neptune Plus multi-collector inductively coupled plasma mass spectrometer (MC-ICP-MS) at ETH Zurich. Samples and standards were measured in 0.5 M HNO₃-0.015 M HF and introduced via a Cetac Aridus II desolvating nebuliser system. Standard sampler and X skimmer cones were used. Measurements were performed in high mass-resolution mode (> 10,000; $m/(m_{0.95}-m_{0.05})$) on the low-mass peak-shoulder to resolve polyatomic interferences. Each sample analysis was bracketed by measurements of the equivalently spiked in-house Ti Alfa Aesar wire standard (Williams et al., 2021) and concentrations for samples and standard were matched within 10 %. Isotope data were acquired in static mode, using 10¹¹ Ω amplifiers for the five stable Ti isotopes (masses 46, 47, 48, 49 and 50) as well as 10¹² Ω amplifiers for ⁴⁴Ca and ⁹⁰Zr⁺⁺, monitored at half mass 45. Beam intensity for ⁴⁸Ti was approximately 40 V. Backgrounds were recorded using pure 0.5 M HNO₃-0.015 M HF solution. Background- and Ca-corrections were performed offline. Data reduction was carried out offline using the signals of ⁴⁶Ti, ⁴⁷Ti, ⁴⁸Ti and ⁴⁹Ti, following the method of Siebert et al. (2001). The Ti isotopic composition is expressed in the delta notation relative to the in-house Ti Alfa Aesar wire standard (Ti-AA Wire) using standard-sample bracketing:

$$\delta^{49}\text{Ti}_{\text{Ti-AA Wire}} (\text{‰}) = \left[\frac{{}^{49}\text{Ti}/{}^{47}\text{Ti}_{\text{Sample}}}{{}^{49}\text{Ti}/{}^{47}\text{Ti}_{\text{Ti-AA Wire}}} - 1 \right] \times 1000$$

The Ti isotope data, denoted as $\delta^{49}\text{Ti}$, are re-scaled to the OL-Ti standard ($\delta^{49}\text{Ti} = \delta^{49}\text{Ti}_{\text{Ti-AA Wire}} + 0.224 \pm 0.017$; Williams et al., 2021). Our intermediate analytical precision was $\pm 0.027 \text{ ‰}$ (2SD), determined for United States Geological Survey (USGS) reference material BHVO-2 ($n = 32$; Table 2). The Ti isotope

composition of BHVO-2 is within uncertainties identical to previous data (e.g. Deng et al., 2019; Johnson et al., 2019; Klaver et al. 2024).

Major element analyses were carried out on fused glasses by wavelength-dispersive X-ray fluorescence spectrometry (WD-XRF) using a PANalytical AXIOS instrument at ETH Zurich. Titanium concentration data reported in Table 2 are derived by isotope dilution as a by-product of the double-spike analyses. Most samples have been previously characterised for their trace element compositions (see Table S1 in the Supplementary Material). Whenever data were not available, trace elements were determined on aliquots of dissolved powders used for Ti isotope analysis using an Element XR ICP-MS at ETH Zurich, as described in Fitzpayne et al. (2023).

4. Results

The Ti isotope compositions of kimberlites from different localities worldwide range from $+0.007 \pm 0.027 \text{ ‰}$ to $+0.173 \pm 0.027 \text{ ‰}$ for $\delta^{49}\text{Ti}$ (Fig. 3, Table 2), where the uncertainty represents the intermediate precision. The observed variation is notably larger than that reported for primitive basalts, including OIBs (Fig. 4). While significant Ti isotope variations exist among different kimberlite provinces, samples from various pipes within a single kimberlite field predominantly display uniform $\delta^{49}\text{Ti}$ values within analytical uncertainties (e.g. $+0.134 \pm 0.027$ to $+0.170 \pm 0.027 \text{ ‰}$, $n = 5$, for the Kimberley cluster in South Africa). Samples from Canada, Greenland, Finland, Russia as well as the Jwaneng (Botswana) and Premier (South Africa) kimberlites mostly have Ti isotope compositions similar to or slightly heavier than basalts. In contrast, the Cretaceous Kimberley kimberlites (South Africa) and the mica-rich Koidu variety (Sierra Leone) as well as samples from Igwisi Hills (Holocene, Tanzania), Murowa (Cambrian, Zimbabwe) and Wajrakarur (Mesoproterozoic, India) display Ti isotope compositions significantly heavier than basalts (Fig. 3, Table 2). We did not observe any systematic variation co-variation between Ti isotopes and major or trace elements across the whole sample suite or within any specific locality (Supplementary Figure S2).

5. Discussion

Mass-dependent Ti isotope variations in mantle-derived magmas may reflect the effects of mineral-melt equilibrium fractionation during partial melting and magmatic differentiation, assimilation of Ti-rich material, or mantle source heterogeneity. Isotopic heterogeneities within the convecting mantle may result from deep subduction of oceanic lithosphere or processes that operated during the early Earth (e.g., White and Hofmann, 1982; Zindler and Hart, 1986; Peters et al., 2018). In addition, melts derived from recycling of subducted (or delaminated) continental material may infiltrate the subcontinental lithosphere hence generating isotopic diversity in metasomatised regions (e.g.,

Hawkesworth et al., 1984; Weiss et al., 2015; Fitzpayne et al., 2019). In the following, we address the potential effects and contributions from (i) fractional crystallisation during kimberlite melt differentiation, (ii) low-degree mantle melting, (iii) compositional variation in the convective mantle source, and (iv) lithospheric mantle assimilation on the Ti isotope characteristics of kimberlites worldwide.

5.1 Fractional crystallisation and kimberlite melt differentiation

5.1.1 Evolution of kimberlite melts and early oxide saturation

Silicate melts may undergo significant Ti isotope fractionation during magma evolution, driven by differences in the bonding environment of Ti in Ti-bearing oxides and the melt they crystallise from. Inter-mineral as well as silicate melt-oxide fractionation factors have been constrained empirically (Greber et al., 2021; Hoare et al., 2022; Johnson et al., 2019, 2023; Mandl 2019; Nie et al., 2021), experimentally (Hoare et al., 2022; Rzehak et al., 2021, 2022), and theoretically (Aarons et al., 2021; Leitzke et al., 2018; Wang et al., 2020), confirming fractional crystallisation of isotopically light Fe-Ti oxides is the major control on Ti isotope fractionation during magmatic differentiation. The studied kimberlites have variable Ti isotope compositions, extending from $\delta^{49}\text{Ti}$ values of $+0.007 \pm 0.027 \text{ ‰}$, which overlap with those of komatiites and primitive basalts (e.g. Deng et al., 2018; Greber et al., 2017b), to distinctly higher values of up to $+0.173 \pm 0.027 \text{ ‰}$ (Figs. 3 and 4, Table 2). The samples contain abundant Ti-bearing phases such as phlogopite/ kinoshitalite mica, as well as various Ti-rich oxides including spinels, perovskite and less common ilmenite–geikielite and rutile (Fig. 2c–f). Early saturation and fractional crystallisation of isotopically light Ti-bearing phases may thus have shifted the Ti isotope composition of the kimberlite magmas towards higher $\delta^{49}\text{Ti}$ values. The first minerals to crystallise in kimberlite melts are olivine and Cr-spinel (e.g. Mitchell, 2008; Soltys et al., 2018a). Except for rare cases (Abersteiner et al., 2019; Soltys et al., 2020), the high ascent rates of kimberlite magmas (up to tens of m/s; Peslier et al., 2008; Sparks et al., 2006), however, prevent significant loss of crystallised minerals via fractional crystallisation, and, thus, magmatic differentiation is generally limited. This is in line with high Mg contents ($\text{MgO} > 25 \text{ wt\%}$, $\text{Mg\#} > 80$; Table S1), abundant xenogenic material (olivine macrocrysts and mantle xenoliths, Fig. 2a–b), and the presence of early crystallised Cr-spinel in all but five of the studied kimberlites.

The Ti budget in kimberlite rocks is dominated by the groundmass phases phlogopite, perovskite and Fe-Ti-rich spinel (\pm less common ilmenite; Fig. 2), which crystallise after magma emplacement in the upper crust (e.g. Abersteiner et al., 2020; Mitchell, 2008; Soltys et al., 2018a). Nevertheless, petrographic studies of kimberlites from Kimberley (South Africa) and Lac de Gras (Canada) indicate early rutile saturation following olivine and Cr-spinel crystallisation (Fedortchouk and Canil, 2004; Soltys

et al., 2018a). Indeed, inclusions of subhedral to euhedral rutile in olivine rims (Fig. 2d) were observed in this study for samples from Wesselton (Kimberley, South Africa), Jwaneng (Botswana), Jericho (Contwoyto, Canada) and Leslie (Lac de Gras, Canada), suggesting early crystallisation from the kimberlite melt. Among these kimberlites, two samples from Wesselton are enriched in heavy Ti isotopes, whereas those from Jwaneng, Jericho and Leslie display Ti isotope data in the range of primitive basalts (Fig. 3, Table 2). Although similar rutile abundance in the samples based on petrographic observations argues against a rutile fractionation effect, below we assess the potential impact of early rutile saturation on the Ti isotope composition of the Kimberley kimberlites.

Difference in the bonding environment between two phases is the first order control on equilibrium isotope fractionation. Titanium in rutile is 6-fold coordinated (Waychunas, 1987), whereas Ti coordination in silicate melts decreases with increasing degree of polymerisation and averages 5.5 in basalts (Farges and Brown, 1997). We assume Rayleigh fractionation and use experimentally derived melt-rutile Ti isotope fractionation factors from Hoare et al. (2022) for kimberlite magma crystallisation temperatures of 1000–1200 °C (Fedortchouk and Canil, 2004). This is a conservative approach since experiments were performed in a haplo-andesitic system (Hoare et al., 2022), whereas kimberlite magmas are highly depolymerised (Moussallam et al., 2016), with a composition transitional between silicate and carbonatite melts (Giuliani et al., 2023; Soltys et al., 2018b). A low degree of polymerisation in carbon-rich and carbonatite melts is further supported by recent Ti isotope data from titanite in carbonatite rocks (Jiang et al., 2024). Considering an initial melt composition with mantle-like $\delta^{49}\text{Ti}$ of +0.02 ‰, the calculation requires removal of >40% of Ti from the melt into rutile to produce high $\delta^{49}\text{Ti}$ of up to \sim +0.17 ‰, as observed for the Kimberley kimberlites (Fig. 5). The Kimberley samples display negative Ti anomalies of variable magnitude ($\text{Ti}/\text{Ti}^* = 0.16\text{--}0.62$, $n = 5$; Fig. 6; with $\frac{\text{Ti}}{\text{Ti}^*} = \frac{\text{Ti}_N}{\sqrt{\text{Sm}_N \times \text{Tb}_N}}$, normalised to primitive mantle (PM) values of McDonough and Sun, 1995), which is a common trait in kimberlites globally (Giuliani et al., 2025; Pearson et al., 2019). The absence of marked negative Nb and Ta anomalies ($\text{Nb}/\text{Nb}^* = 1.11\text{--}1.65$, $\text{Ta}/\text{Ta}^* = 0.80\text{--}2.08$; with $\frac{\text{Nb}}{\text{Nb}^*} = \frac{\text{Nb}_N}{\sqrt{\text{Th}_N \times \text{La}_N}}$ and $\frac{\text{Ta}}{\text{Ta}^*} = \frac{\text{Ta}_N}{\sqrt{\text{Th}_N \times \text{La}_N}}$) in the Kimberley kimberlites, however, strongly argues against significant rutile fractionation.

5.1.2 Titanium isotope composition of differentiated kimberlites

Magma stalling at shallow crustal levels may result in kimberlite melt differentiation via fractional crystallisation (e.g. Sparks, 2013; Zurevinski and Mitchell, 2011). To assess the extent of Ti isotope fractionation during differentiation of kimberlite melts, some evolved samples were analysed for their Ti isotope composition. Kimberlites from four of the five differentiated samples, namely those from the Kuusamo area (KV001, KP-104; Finland), the Wesselton Water Tunnel and Benfontein sills (BUSK-1, WWTS-P3; Kimberley, South Africa) (Table 1) have notably low MgO (≤ 20 wt%) and high CaO contents

(> 15 wt%; Table S1) compared to kimberlites elsewhere including other samples from the same localities. The scarcity of xenogenic mantle material and the almost complete absence of Cr-spinel further indicate that these kimberlites experienced crystal-liquid fractionation (Abersteiner et al., 2019; Dalton et al., 2019; Le Roex et al., 2003). The Kuusamo kimberlites yield $\delta^{49}\text{Ti}$ values of $+0.053 \pm 0.027$ and $+0.098 \pm 0.027$ ‰ (Table 2). The lower TiO_2 contents and relative enrichment in K_2O and incompatible trace elements may indicate the slightly heavier Ti isotope composition of sample KV001 compared to KP-104 is related to a higher degree of differentiation (Tables 2 and S1). In contrast, highly evolved samples from the Benfontein and Wesselton Water Tunnel sills (Kimberley) display $\delta^{49}\text{Ti}$ values identical within analytical uncertainty to those of undifferentiated kimberlites from the Kimberley area (Table 2). These results suggest magmatic differentiation and fractional crystallisation of Ti-bearing phases likely had a minor effect on the Ti isotope compositions of the studied kimberlites. The overall indistinguishable although elevated $\delta^{49}\text{Ti}$ values of differentiated and primitive kimberlites from various pipes/sills in the Kimberley cluster (Fig. 3) further implies that the process that affected their Ti isotope compositions had to be common to the Kimberley melts and preceded their emplacement.

5.2 Source processes

5.2.1 Effects of partial melting of a carbonated mantle

Kimberlites in this work and globally (Giuliani et al., 2025) predominantly display negative Ti anomalies of variable magnitude (Fig. 6). Based on petrographic observations and the lack of negative Nb-Ta anomalies, these anomalies are likely unrelated to fractional crystallisation of Ti-rich phases such as rutile and ilmenite during kimberlite magma ascent. The negative Ti-anomalies could reflect partial melting of CO_2 -bearing peridotites in the presence of a Ti-bearing phase (Dasgupta et al., 2009; Giuliani et al., 2025), or the signature of the kimberlite mantle source (e.g. Le Roex et al., 2003). Previous studies suggested negligible Ti isotope fractionation during partial melting of a 4-phase peridotitic mantle (i.e. containing olivine, orthopyroxene, clinopyroxene and garnet) with a peridotite-melt fractionation factor close to unity (Anguelova et al., 2022; Deng et al., 2018; Hoare et al., 2022; Millet et al., 2016). Kimberlite melts are thought to derive from depths of ~ 150 – 250 km and temperatures of $\sim 1450 \pm 50$ °C by low-degree melting (<1%) of a 4-phase carbonated peridotite mantle source (Giuliani et al., 2023; Stamm and Schmidt, 2017). At such P-T conditions, Ti is dominantly stored in clinopyroxene and garnet. Due to a reduced TiO_2 solubility in carbonatitic and carbonated silicate melts (Dasgupta et al., 2009), akin to kimberlite primary melts (e.g. Nielsen and Sand, 2008; Russell et al., 2012; Soltys et al., 2018b), equilibration of such low-degree melts with clinopyroxene and garnet may produce negative Ti anomalies, but is unlikely to fractionate Ti isotopes (Anguelova et al., 2022; Hoare et al., 2022; Rzehak et al., 2021).

5.2.2 Source heterogeneity

Geochemically enriched Sr-Nd-Hf isotope signatures of Mesozoic and Cenozoic kimberlites from southern Africa, western Canada, and other regions suggest that the source of kimberlites was widely contaminated by deeply subducted crustal material in recent times (<250 Ma, Woodhead et al., 2019; Giuliani et al., 2021). Decoupled Nd-Hf isotope compositions in Precambrian kimberlites (e.g. Premier, South Africa; Murowa, Zimbabwe; Kaavi-Kuopio, Finland; Dalton et al., 2022; Tappe et al., 2020a; Giuliani et al., 2025), argue for recycling of ancient oceanic crust also in the source region of some older kimberlites. Recycled MORB or OIB-type oceanic crust (\pm sediments) is also invoked to explain radiogenic isotope variability in OIBs (e.g. Chauvel et al., 1992; Elliott et al., 2007; Rapp et al., 2008). Unlike kimberlites, primitive OIBs display homogeneous Ti isotope compositions indistinguishable or marginally heavier than MORBs (Fig. 4; Millet et al., 2016; Deng et al., 2023). Kimberlite magmas, however, represent very small-degree melts (\ll 1%) and isotopic heterogeneities are, hence, less diluted by the more extensive melting of ambient, depleted mantle that is involved in genesis of OIBs and MORBs.

The examined kimberlites display $\delta^{49}\text{Ti}$ values ranging from ~ 0 ‰ to enriched in heavy Ti isotopes (Fig. 3, Table 2). Sediments show heavy Ti isotope compositions compared to the mantle (e.g. Greber et al., 2017a). An estimate of the Ti isotope composition of the upper continental crust can be derived from marine shales (Deng et al., 2019; Greber et al., 2017a) and yield an average $\delta^{49}\text{Ti}$ value of $+0.184 \pm 0.069$ ‰ (1SD, $n = 88$; Anguelova et al., 2022). In addition, hydrodynamic sorting may enrich sediments derived from mafic lithologies in isotopically heavy Ti (Klaver et al., 2021). Hence, subducted sedimentary material has the potential to generate high $\delta^{49}\text{Ti}$ domains within the convective mantle. While kimberlites from Kimberley as well samples from the Igwisi Hills, Koidu and Wajrakarur kimberlite fields lie, within uncertainty, on a theoretical $\delta^{49}\text{Ti}$ mixing line between the primitive mantle and terrigenous sediments, the addition of $\sim 50\%$ sediment-derived Ti is required to generate high $\delta^{49}\text{Ti}$ values of $\sim +0.15$ ‰ (Fig. S3). Such high contribution from sedimentary material is, however, not supported by radiogenic isotope systematics, including those of an element with similar geochemical behaviour like Hf (Fig. S4, Table S1). The oceanic crust, on the other hand, is characterised by higher Ti contents (1.53 wt% TiO_2 , avg. MORB; Gale et al., 2013) and less extreme radiogenic isotope compositions compared to the continental crust and sediments. Eclogites and primitive MORBs, however, display Ti isotopes compositions of ~ 0 ‰ (e.g. Deng et al., 2018; Millet et al., 2016). While mid-ocean ridge and intraplate differentiates may be strongly enriched in isotopically heavy Ti (Deng et al., 2019; Hoare et al., 2020), evolved lithologies would likely account for a small fraction of the subducted oceanic crust. Hence, the Ti isotope composition of the bulk of subducted oceanic crust material is not expected to significantly deviate from ~ 0 ‰ and cannot contribute towards increasing

the Ti isotope composition of kimberlites. In alternative, melts derived from partial melting of subducted oceanic crust or sediments may have substantially higher $\delta^{49}\text{Ti}$ than their protoliths if produced in presence of residual Ti-bearing oxide minerals or amphibole (Klaver et al., 2024; Spencer et al., 2024; Zhao et al., 2025). Percolation of these melts in the convecting mantle could generate metasomatic domains with Ti isotope values sufficiently high to match the compositions of kimberlites. Yet, these melts are likely to be limited to supra-subduction environments, which are not applicable to the genesis of kimberlites in intraplate settings far away from subduction zones (Giuliani et al., 2023). In summary, it appears unlikely that the elevated $\delta^{49}\text{Ti}$ values observed in some kimberlites were inherited from their mantle sources, even though source heterogeneity and, specifically, contribution by subducted sedimentary material might have locally contributed.

5.3 Assimilation of enriched lithospheric mantle

During ascent, kimberlite magmas may entrain and assimilate lithospheric mantle material (Bussweiler et al., 2016; Russell et al., 2012; Soltys et al., 2016), which strongly shapes the composition of the evolving kimberlite melt (Dalton et al., 2020; Giuliani et al., 2020; Xu et al., 2021; Howarth et al., 2022). Conversely, while there is petrographic and geochemical evidence of interaction with crustal debris in several kimberlites, this effect appears to be spatially limited to just few cm from the entrained fragments and is therefore important only in kimberlites containing abundant crustal material (Fulop et al., 2018; Nyiazova et al., 2022). This is not the case for our samples, which are devoid of obvious crustal contamination. The entrained mantle cargo includes variably depleted and re-enriched (i.e. metasomatised) subcontinental lithospheric mantle (SCLM) material beneath cratons (e.g. Brey and Shu, 2018; Pearson and Wittig, 2014; Simon et al., 2007). While the SCLM is predominantly composed of peridotite (i.e. dunite, harzburgite and lherzolite), xenoliths with metasomatic assemblages such as MARID (mica-amphibole-rutile-ilmenite-diopside) rocks (Erlank et al., 1987; Fitzpayne et al., 2019; Gregoire et al., 2002; Konzett et al., 1998), and the formation of potassic–ultrapotassic magmas (Becker and Le Roex, 2006; Chalapathi Rao et al., 2013; Fraser et al., 1985; Mitchell, 2020) indicate the local presence of strongly enriched metasomes within the cratonic lithosphere. Assimilation of diverse mantle material could, therefore, potentially contribute to the observed inter-province Ti isotope variability in kimberlite rocks.

Contribution from Ti-poor refractory peridotite will not affect the Ti isotope budget of primary kimberlite melts (≥ 0.5 wt% of TiO_2 ; Soltys et al., 2018b and references therein). In contrast, metasomatised mantle domains may be enriched in Ti with highly variable Ti isotope compositions (Anguelova et al., 2022). In addition, ultrapotassic rocks originating from strongly metasomatised

domains within the lithospheric mantle display heavy Ti isotope compositions of up to $\sim +0.3\%$ (Anguelova et al., 2022; Fig. 4).

Viljoen et al. (2022) and Fitzpayne et al. (2023) recently suggested that the strong enrichment in mica in kimberlites from Sierra Leone (including Koidu, measured in our study) stems from interaction with strongly metasomatised phlogopite-bearing lithospheric mantle. A similar model was previously proposed to explain the variations in mica contents (from kimberlites to lamproites) across the Wajrakarur field (Shaikh et al., 2018; Sarkar et al., 2021). Therefore, the micaceous nature of kimberlites can be employed as a first-order approximation of the interaction between asthenospheric kimberlite melts and metasomatised lithospheric mantle. Variably micaceous kimberlites examined in this work include samples from Koidu ($+0.141 \pm 0.027\%$, $n = 1$), Wajrakarur ($+0.154 \pm 0.027\%$, $n = 2$), and Kimberley ($+0.134 \pm 0.027\%$ to $+0.173 \pm 0.027\%$, $n = 5$ including a sample from the nearby Jagersfontein cluster; Table 2). All these samples exhibit elevated $\delta^{49}\text{Ti} > +0.1\%$. Evidence for an enriched mica-bearing lithospheric mantle beneath the southwestern Kaapvaal (South Africa) and eastern Dharwar cratons (India) is provided by the occurrence of olivine-lamproites in these regions, which are temporally associated with kimberlites (e.g. Smith et al., 1994; Pandey and Rao, 2020; Sarkar et al., 2023). In addition, abundant MARID and other phlogopite-rich xenoliths occur in both kimberlites and olivine-lamproites in the southwestern Kaapvaal (e.g. Mitchell, 1995; Fitzpayne et al., 2018, 2019), a region that is well known for extensive mica-rich metasomatism of the lithospheric roots (Erlank et al., 1987). While the Ti isotope composition of the lithospheric mantle beneath the Wajrakarur and Koidu kimberlite fields is unconstrained, metasomatised domains within the SCLM beneath the Kaapvaal craton are enriched in heavy Ti isotopes: olivine-lamproites and a kimberlite-hosted MARID display $\delta^{49}\text{Ti}$ values of $+0.129 \pm 0.029\%$ ($n = 3$) and $+0.128 \pm 0.012\%$, respectively (Anguelova et al., 2022, Table S2). Although these few samples are unlikely to catch the whole extent of Ti isotope variations of metasomatised domains in the SCLM, they demonstrate the presence of isotopically heavy Ti in the lithospheric mantle that interacts with traversing kimberlite melts. Therefore, it appears reasonable that kimberlite interaction with micaceous sub-lithospheric components containing isotopically heavy Ti contribute to elevating the Ti isotope compositions of micaceous kimberlites.

The Mg# [= $\text{Mg}/(\text{Mg}+\text{Fe})$ in molar proportions] of olivine represents a robust tool to assess the extent of interaction between asthenospheric kimberlite melts and lithospheric mantle wall rocks (Dalton et al., 2020; Giuliani et al., 2020; Tovey et al., 2021). Higher extents of interaction with Fe-Ti-rich metasomatised lithospheric mantle result in lower Mg# in magmatic olivine as well as higher concentrations of groundmass mica and Fe-Ti oxide minerals in kimberlites (Lim et al., 2018; Giuliani et al., 2020; Viljoen et al., 2022). Importantly, recent work indicates that this process also affects the Ti concentrations of magmatic olivine and hence of kimberlite melts (Howarth et al., 2022). The Ti isotope

data of kimberlites overall correlates with the Mg# of magmatic olivine (Fig. 7). While noting that not all samples are associated with olivine compositions, kimberlites with olivine Mg# ≥ 90 (Lac de Gras, Contwoyto, Slave Craton) have low $\delta^{49}\text{Ti}$ values (≤ 0.05 ‰), which are typical of primitive basalts (Fig. 7). This is in line with the depleted peridotitic SCLM presumed to be entrained by kimberlites emplaced in the central and norther parts of the Slave craton (Griffin et al., 1999). The remaining kimberlites show a progressively larger scatter of Ti isotope composition with decreasing Mg#. Four of these samples (Premier, Pipe 14, Poiskovaya and Majuagaa) exhibit clear evidence of Ti-rich oxide mineral accumulation based on petrographic observations and $\text{Ti}/\text{Ti}^* > 1$. Oxide mineral accumulation decreases the $\delta^{49}\text{Ti}$ composition compared to pristine melt values because oxides have substantially lower $\delta^{49}\text{Ti}$ than their equilibrium melt (see Section 5.1). Excluding these four samples, a remarkably robust linear trend becomes apparent, with kimberlite $\delta^{49}\text{Ti}$ and olivine Mg# being inversely correlated ($R^2 = 0.70$; $n = 10$, Fig. 7). This trend underpins a strong lithospheric control on the Ti isotope composition of kimberlite magmas, especially for samples with elevated Ti isotope compositions. Considering the limited knowledge of Ti isotope systematic in metasomatised mantle rocks and the likely variations occurring across the examined localities, it is currently impossible to quantitatively estimate the details of this interaction process. While mineral assimilation appears to be likely, incongruent melting of Ti-rich phases such as mica (Sarkar et al., 2022) and isotopic exchange between melt and entrained wall rock material are also plausible.

6. Conclusions

Kimberlites from 15 kimberlite fields worldwide with emplacement ages from ~ 1.15 Ga to the Holocene display variable $\delta^{49}\text{Ti}$ values ranging from basalt-like ($+0.007 \pm 0.027$ ‰) compositions to enrichments in heavy Ti isotopes ($+0.173 \pm 0.027$ ‰). The observed $\delta^{49}\text{Ti}$ variation of ~ 0.17 ‰ is larger than that identified in primitive OIBs, for which a common origin to kimberlites is suggested based on similar radiogenic isotope systematics. Large inter-province $\delta^{49}\text{Ti}$ variations contrast with homogeneous intra-province Ti isotope compositions. The identical $\delta^{49}\text{Ti}$ values, within uncertainties, of primitive and highly differentiated kimberlites from a single kimberlite field suggest that the heavy Ti isotope compositions are not the result of low-pressure crystal-liquid fractionation. This contrasts with the Ti isotope fractionation trends observed in the majority of magmatic rocks and supports late crystallisation of the main Ti carriers upon kimberlite magma emplacement within the upper crust. It may further entail that Ti coordination in highly depolymerised carbonated silicate melts is high and similar to that in mantle minerals, limiting isotopic fractionation. Consequently, Ti isotope fractionation during low-degree melting of a carbonated deep mantle source is considered unlikely. Binary mixing models suggest that contribution by subducted material cannot explain the Ti (and Hf) isotope systematics of the examined

samples assuming realistic contributions of sedimentary material. Heavy Ti isotope compositions are found in kimberlites with high mica contents and low Mg# in olivine, both indicative of extensive interaction of primary kimberlite melts with strongly metasomatised, Fe-Ti-rich lithospheric mantle. These observations and the remarkable inverse correlation between $\delta^{49}\text{Ti}$ and olivine Mg# provide evidence for a dominant role of the metasomatised lithospheric mantle in producing the high $\delta^{49}\text{Ti}$ values recorded by some of the kimberlites. However, details of this interaction process remain obscure, including assimilation and the potential role of incongruent melting of entrained material such as Ti-rich mica. This work highlights the potential role of Ti isotopes as tracers of assimilation of metasomatised lithospheric mantle, hence expanding the application of this novel isotopic tool to the investigation of mantle-derived magmas.

Acknowledgements

We would like to thank Troels Nielsen, Roger Mitchell, Hugh O'Brien, Zdislav Spetsius, Janet Hergt, Jon Woodhead, Richard Brown, Jock Robey, Petra Diamonds, Dominion Diamonds, Sierra Diamonds, De Beers Group, and Rio Tinto for providing access to the samples examined in this study. Lydia Zehnder (ETH Zurich) is acknowledged for her support with the XRF-analysis and Angus Fitzpayne (ETH Zurich) for helping with the trace-element analysis. Reviews from Sebastian Kommescher and 2 anonymous referees, and additional editorial input by Tomas Magna are duly acknowledged. This project was founded by the Swiss National Science Foundation (Project 2 00020_179129 and 200021_208079 to MS).

CRedit

Merislava Anguelova: Conceptualisation, Investigation, Writing – original draft

Andrea Giuliani: Conceptualisation, Investigation, Writing – original draft

Manuela A. Fehr: Writing – review and editing

Maria Schönbächler: Conceptualisation, Funding acquisition, Writing – review and editing

Data Availability

During the review process, the data is provided in the Supplementary Information. Upon publication, the data will be made available via the Research Collection of ETH Zurich (<https://doi.org/10.3929/ethz-b-000727482>).

Appendix A. Supplementary Material

The supplementary document includes: (i) a description of the geological context of the studied kimberlites, (ii) Ti isotope data of olivine-lamproites, (iii) and details on the mixing model constraints. It also provides major and trace element compositions, age data, and, where available, Nd and Hf isotope data for the studied kimberlites. Additionally, literature Ti isotope data for mantle-derived magmas shown in Fig. 4 are provided.

Journal Pre-proofs

References

- Aarons S. M., Dauphas N., Blanchard M., Zeng H., Nie N. X., Johnson A. C., Greber N. D. and Hopp T. (2021) Clues from *ab initio* calculations on titanium isotopic fractionation in tholeiitic and calc-alkaline magma series. *ACS Earth Space Chem.* **5**, 2466–2480.
- Aarons S. M., Reimink J. R., Greber N. D., Heard A. W., Zhang Z. and Dauphas N. (2020) Titanium isotopes constrain a magmatic transition at the Hadean-Archean boundary in the Acasta Gneiss Complex. *Sci. Adv.* **6**, eabc9959.
- Abersteiner A., Kamenetsky V.S., Goemann K., Giuliani A., Howarth G.H., Castillo-Oliver M., Thompson J., Kamenetsky M. and Cherry A. (2019) Composition and emplacement of the Benfontein kimberlite sill complex (Kimberley, South Africa): Textural, petrographic and melt inclusion constraints. *Lithos* **324**, 297–314.
- Abersteiner A., Kamenetsky V.S., Goemann K., Kjarsgaard B.A., Fedortchouk Y., Ehrig K. and Kamenetsky M. (2020) Evolution of kimberlite magmas in the crust: A case study of groundmass and mineral-hosted inclusions in the Mark kimberlite (Lac de Gras, Canada). *Lithos* **372**, 105690.
- Angelova M., Fehr M.A., Takazawa E. and Schönbächler M. (2022) Titanium isotope heterogeneity in the Earth's mantle: a case study of the Horoman peridotite massif. *Geochim. Cosmochim. Acta* **335**, 356–368.
- Angelova M., Vilela N., Kommescher S., Greber N.D., Fehr M.A. and Schönbächler M. (2024) Constraining the mass-dependent Ti isotope composition of the chondritic reservoir—An inter-laboratory comparison study. *Geochim. Cosmochim. Acta* **372**, 171–180.
- Antonelli M.A., Giuliani A., Wang Z., Wang M., Zhou L., Feng L., Li M., Zhang Z., Liu F. and Drysdale R.N. (2023) Subducted carbonates not required: Deep mantle melting explains stable Ca isotopes in kimberlite magmas. *Geochim. Cosmochim. Acta* **348**, 410–427.
- Aulbach S., Höfer H.E. and Gerdes A. (2019) High-Mg and low-Mg mantle eclogites from Koidu (West African Craton) linked by Neoproterozoic ultramafic melt metasomatism of subducted Archean plateau-like oceanic crust. *J. Petrol.* **60**, 723–754.
- Becker M. and Roex A.P.L. (2006) Geochemistry of South African on- and off-craton, Group I and Group II kimberlites: petrogenesis and source region evolution. *J. Petrol.* **47**, 673–703.
- Brey G.P. and Shu Q. (2018) The birth, growth and ageing of the Kaapvaal subcratonic mantle. *Miner. Petrol.* **112**, 23–41.
- Bussweiler Y., Stone R.S., Pearson D.G., Luth R.W., Stachel T., Kjarsgaard B.A. and Menzies, A. (2016) The evolution of calcite-bearing kimberlites by melt-rock reaction: evidence from polymineralic inclusions within clinopyroxene and garnet megacrysts from Lac de Gras kimberlites, Canada. *Contrib. Mineral. Petrol.* **171**, 1–25.

- Chauvel C., Hofmann A.W. and Vidal P. (1992) HIMU-EM: the French Polynesian connection. *Earth Planet. Sci. Lett.* **110**, 99–119.
- Dalton H., Giuliani A., Hergt J., Phillips D., O'Brien H., Ballmer M.D., Maas R. and Woodhead J. (2022) Geodynamic and isotopic constraints on the genesis of kimberlites, lamproites and related magmas from the Finnish segment of the Karelian craton. *Geochem. Geophys. Geosyst.* **23**, e2021GC010324.
- Dalton H., Giuliani A., O'Brien H., Phillips D. and Hergt J. (2020) The role of lithospheric heterogeneity on the composition of kimberlite magmas from a single field: The case of Kaavi-Kuopio, Finland. *Lithos* **354**, 105333.
- Dalton H., Giuliani A., O'Brien H., Phillips D., Hergt J. and Maas R. (2019) Petrogenesis of a hybrid cluster of evolved kimberlites and ultramafic lamprophyres in the Kuusamo area, Finland. *J. Petrol.* **60**, 2025–2050.
- Dasgupta R., Hirschmann M.M., McDonough W.F., Spiegelman M. and Withers A.C. (2009) Trace element partitioning between garnet lherzolite and carbonatite at 6.6 and 8.6 GPa with applications to the geochemistry of the mantle and of mantle-derived melts. *Chem. Geol.* **262**, 57–77.
- Deng Z., Chaussidon M., Savage P., Robert F., Pik R. and Moynier F. (2019) Titanium isotopes as a tracer for the plume or island arc affinity of felsic rocks. *Proc. Natl. Acad. Sci.* **116**, 1132–1135.
- Deng Z., Moynier F., Sossi P. and Chaussidon M. (2018) Bridging the depleted MORB mantle and the continental crust using titanium isotopes. *Geochem. Perspect. Lett.* **9**, 11–15.
- Deng Z., Schiller M., Jackson M.G., Millet M.-A., Pan L., Nikolajsen K., Saji N.S., Huang D. and Bizzarro M. (2023) Earth's evolving geodynamic regime recorded by titanium isotopes. *Nature* **621**, 100–104.
- Dymshits A.M., Sharygin I.S., Malkovets V.G., Yakovlev I.V., Gibsher A.A., Alifirova T.A., Vorobei S.S., Potapov S.V. and Garanin V.K. (2020) Thermal state, thickness, and composition of the lithospheric mantle beneath the Upper Muna Kimberlite Field (Siberian Craton) constrained by clinopyroxene xenocrysts and comparison with Daldyn and Mirny Fields. *Minerals* **10**, 549.
- Elliott T., Blichert-Toft J., Heumann A., Koetsier G. and Forjaz V. (2007) The origin of enriched mantle beneath São Miguel, Azores. *Geochim. Cosmochim. Acta* **71**, 219–240.
- Erlank A., Waters F.G., Hawkesworth, C. J. and Haggerty S. (1987) Evidence for mantle metasomatism in peridotite nodules from the Kimberley pipes, South Africa. *In. Mantle metasomatism*, 221–311.
- Farges F. and Brown G.E. (1997) Coordination chemistry of titanium (IV) in silicate glasses and melts: IV. XANES studies of synthetic and natural volcanic glasses and tektites at ambient temperature and pressure. *Geochim. Cosmochim. Acta* **61**, 1863–1870.
- Fedortchouk Y. and Canil D. (2004) Intensive variables in kimberlite magmas, Lac de Gras, Canada and implications for diamond survival. *J. Petrol.* **45**, 1725–1745.

- Fitzpayne A., Giuliani A., Hergt J., Phillips D. and Janney P. (2018) New geochemical constraints on the origins of MARID and PIC rocks: Implications for mantle metasomatism and mantle-derived potassic magmatism. *Lithos* **318**, 478–493.
- Fitzpayne A., Giuliani A., Hergt J., Woodhead J.D. and Maas R. (2020) Isotopic analyses of clinopyroxenes demonstrate the effects of kimberlite melt metasomatism upon the lithospheric mantle. *Lithos* **370**, 105595.
- Fitzpayne A., Giuliani A., Howarth G.H., Peters B.J., Fehr M.A. and Maas R. (2023) Major-, trace-element and Sr-Nd-Hf isotope geochemistry of diamondiferous dykes from Tonguma and Koidu, Sierra Leone: highly micaceous kimberlites formed by assimilation of metasomatised lithospheric mantle rocks. *Chem. Geol.* **630**, 121475.
- Fitzpayne A., Giuliani A., Maas R., Hergt J., Janney P. and Phillips D. (2019) Progressive metasomatism of the mantle by kimberlite melts: Sr–Nd–Hf–Pb isotope compositions of MARID and PIC minerals. *Earth Planet. Sci. Lett.* **509**, 15–26.
- Fraser K., Hawkesworth C., Erlank A., Mitchell R. and Scott-Smith B. (1985) Sr, Nd and Pb isotope and minor element geochemistry of lamproites and kimberlites. *Earth Planet. Sci. Lett.* **76**, 57–70.
- Fulop A., Kopylova M., Kurszlaukis S., Hilchie L., Ellemers P. and Squibb C. (2018) Petrography of Snap Lake kimberlite dyke (Northwest Territories, Canada) and its interaction with country rock granitoids. *J. Petrol.* **59**, 2493–2518.
- Gale A., Dalton C.A., Langmuir C.H., Su Y. and Schilling J.G. (2013) The mean composition of ocean ridge basalts. *Geochem. Geophys. Geosyst.* **14**, 489–518.
- Giuliani A., Dalton H. and Pearson D.G. (2025) Kimberlites: the deepest geochemical probes of Earth, *Treatise of Geochemistry*, 3rd edition: Earth's Interior, 159–230.
- Giuliani A., Drysdale R.N., Woodhead J.D., Planavsky N.J., Phillips D., Hergt J., Griffin W.L., Oesch S., Dalton H. and Davies G.R. (2022) Perturbation of the deep-Earth carbon cycle in response to the Cambrian Explosion. *Sci. Adv.* **8**, eabj1325.
- Giuliani A., Jackson M.G., Fitzpayne A. and Dalton H. (2021) Remnants of early Earth differentiation in the deepest mantle-derived lavas. *Proc. Natl. Acad. Sci.* **118**.
- Giuliani A. and Pearson D.G. (2019) Kimberlites: from deep earth to diamond mines. *Elements* **15**, 377–380.
- Giuliani A., Pearson D.G., Soltys A., Dalton H., Phillips D., Foley S.F., Lim E., Goemann K., Griffin W.L. and Mitchell R.H. (2020) Kimberlite genesis from a common carbonate-rich primary melt modified by lithospheric mantle assimilation. *Sci. Adv.* **6**, eaaz0424.
- Giuliani A., Schmidt M.W., Torsvik T.H. and Fedortchouk Y. (2023) Genesis and evolution of kimberlites. *Nat. Rev. Earth Environ.* **4**, 738–753..

- Greber N. D., Dauphas N., Bekker A., Ptáček M. P., Bindeman I. N. and Hofmann A. (2017a) Titanium isotopic evidence for felsic crust and plate tectonics 3.5 billion years ago. *Science* **357**, 1271–1274.
- Greber N. D., Dauphas N., Puchtel I. S., Hofmann B. A. and Arndt N. T. (2017b) Titanium stable isotopic variations in chondrites, achondrites and lunar rocks. *Geochim. Cosmochim. Acta* **213**, 534–552.
- Greber N. D., Pettke T., Vilela N., Lanari P. and Dauphas N. (2021) Titanium isotopic compositions of bulk rocks and mineral separates from the Kos magmatic suite: Insights into fractional crystallization and magma mixing processes. *Chem. Geol.* **578**, 120303.
- Grégoire M., Bell D. and Le Roex A. (2002) Trace element geochemistry of phlogopite-rich mafic mantle xenoliths: their classification and their relationship to phlogopite-bearing peridotites and kimberlites revisited. *Contrib. Mineral. Petrol.* **142**, 603–625.
- Griffin W., Doyle B., Ryan C., Pearson N., Suzanne Y.O.R., Davies R., Kivi K., Van Achterbergh E. and Natapov L. (1999) Layered mantle lithosphere in the Lac de Gras area, Slave craton: composition, structure and origin. *J. Petrol.* **40**, 705–727.
- Griffin W., Doyle B., Ryan C., Pearson N., Suzanne Y.O.R., Davies R., Kivi K., Van Achterbergh E. and Natapov L. (1999) Layered mantle lithosphere in the Lac de Gras area, Slave craton: composition, structure and origin. *J. Petrol.* **40**, 705–727.
- Griffin W., O'reilly S.Y., Afonso J.C. and Begg G. (2009) The composition and evolution of lithospheric mantle: a re-evaluation and its tectonic implications. *J. Petrol.* **50**, 1185–1204.
- Hawkesworth C., Rogers N., Van Calsteren P. and Menzies M. (1984) Mantle enrichment processes. *Nature* **311**, 331–335.
- Hoare L., Klaver M., Muir D.D., Klemme S., Barling J., Parkinson I.J., Lissenberg C.J. and Millet M.-A. (2022) Empirical and experimental constraints on Fe-Ti oxide-melt titanium isotope fractionation factors. *Geochim. Cosmochim. Acta* **326**, 253–272.
- Hoare L., Klaver M., Saji N.S., Gillies J., Parkinson I.J., Lissenberg C.J. and Millet M.-A. (2020) Melt chemistry and redox conditions control titanium isotope fractionation during magmatic differentiation. *Geochim. Cosmochim. Acta* **282**, 38–54.
- Howarth G.H., Giuliani A., Soltys A. and Bussweiler Y. (2022) Compositional variations in primitive kimberlite melts and entrained mantle cargo from a global survey of trace element compositions in kimberlite olivine. *J. Petrol* **63**, egac062.
- Hunter R.H. and Taylor L.A. (1982) Instability of garnet from the mantle: glass as evidence of metasomatic melting. *Geology* **10**, 617–620.
- Irvine G.J., Pearson D.G., Kjarsgaard B., Carlson R., Kopylova M. and Dreibus G. (2003) A Re–Os isotope and PGE study of kimberlite-derived peridotite xenoliths from Somerset Island and a comparison to the Slave and Kaapvaal cratons. *Lithos* **71**, 461–488.

- Jackson M.G. and Jellinek A.M. (2013) Major and trace element composition of the high $^3\text{He}/^4\text{He}$ mantle: Implications for the composition of a nonchondritic Earth. *Geochem. Geophys. Geosyst.* **14**, 2954–2976.
- Jiang X., Chen X., Jiang S., Hoare L., Zhang W., Lian D., Cai P., Xu Y. and Liu H. (2024) Immiscibility of carbonatitic and alkaline silicate melts from an evolved ultramafic magma: titanite geochronology and in-situ TiNd isotope insights. *Chem. Geol.* **670**, 122433.
- Johnson A.C., Aarons S.M., Dauphas N., Nie N.X., Zeng H., Helz R.T., Romaniello, S.J. and Anbar, A.D. (2019) Titanium isotopic fractionation in Kilauea Iki lava lake driven by oxide crystallization. *Geochim. Cosmochim. Acta* **264**, 180–190.
- Johnson A.C., Zhang Z.J., Dauphas N., Rudnick R.L., Foden J.D. and Toc M. (2023) Redox and mineral controls on Fe and Ti isotopic fractionations during calc-alkaline magmatic differentiation. *Geochim. Cosmochim. Acta* **355**, 1–12.
- Khan S., Dongre A., Viljoen F., Li Q.L. and Le Roux P. (2019) Petrogenesis of lamprophyres synchronous to kimberlites from the Wajrakarur kimberlite field: implications for contrasting lithospheric mantle sources and geodynamic evolution of the eastern Dharwar Craton of southern India. *Geol. J.* **54**, 2994–3016.
- Kjarsgaard B.A., de Wit M., Heaman L.M., Pearson D.G., Stiefenhofer J., Januszczak N. and Shirey S.B. (2022) A review of the geology of global diamond mines and deposits. *Rev. Mineral. Geochem.* **88**, 1–117.
- Klaver M., MacLennan S.A., Ibañez-Mejía M., Tissot F.L., Vroon P.Z. and Millet M.-A. (2021) Reliability of detrital marine sediments as proxy for continental crust composition: The effects of hydrodynamic sorting on Ti and Zr isotope systematics. *Geochim. Cosmochim. Acta* **310**, 221–239.
- Klaver M., Yogodzinski G., Albert C., Camejo-Harry M., Elburg M., Hoernle K., Macpherson C., Nowell G., Rushmer T. and Williams H. (2024) Widespread slab melting in modern subduction zones. *Earth Planet. Sci. Lett.* **626**, 118544.
- Kommacher S., Kurzweil F., Fonseca R.O., Rzehak L.J.A., Hohl S., Kirchenbaur M., Schuth S., Sprung P. and Münker C. (2023) Mineralogical controls on the Ti isotope composition of subduction zone magmas. *Geochem. Geophys. Geosyst.* **24**, e2022GC010840
- Konzett J., Armstrong R.A., Sweeney R.J. and Compston W. (1998) The timing of MARID metasomatism in the Kaapvaal mantle: an ion probe study of zircons from MARID xenoliths. *Earth Planet. Sci. Lett.* **160**, 133–145.
- Le Roex A.P., Bell D.R. and Davis P. (2003) Petrogenesis of group I kimberlites from Kimberley, South Africa: evidence from bulk-rock geochemistry. *J. Petrol.* **44**, 2261–2286.

- Leitzke F., Fonseca R., Göttlicher J., Steininger R., Jahn S., Prescher C. and Lagos M. (2018) Ti K-edge XANES study on the coordination number and oxidation state of Titanium in pyroxene, olivine, armalcolite, ilmenite, and silicate glass during mare basalt petrogenesis. *Contrib. Mineral. Petrol.* **173**, 1–17.
- Lim E., Giuliani A., Phillips D. and Goemann K. (2018) Origin of complex zoning in olivine from diverse, diamondiferous kimberlites and tectonic settings: Ekati (Canada), Alto Paranaíba (Brazil) and Kaalvallei (South Africa). *Mineral. Petrol.* **112**, 539–554.
- Mandl M.B. (2019) Titanium isotope fractionation on the Earth and Moon: Constraints on magmatic processes and Moon formation. Doctoral Thesis, ETH Zürich.
- McDonough W.F. and Sun S.-S. (1995) The composition of the Earth. *Chem. Geol.* **120**, 223–253.
- Millet M.-A. and Dauphas N. (2014) Ultra-precise titanium stable isotope measurements by double-spike high resolution MC-ICP-MS. *J. Anal. At. Spectrom.* **29**, 1444–1458.
- Millet M.-A., Dauphas N., Greber N.D., Burton K.W., Dale C.W., Debret B., Macpherson C.G., Nowell G.M. and Williams H.M. (2016) Titanium stable isotope investigation of magmatic processes on the Earth and Moon. *Earth Planet. Sci. Lett.* **449**, 197–205.
- Mitchell R.H. (1995) Kimberlites and orangeites, Kimberlites, Orangeites, and Related Rocks. Springer, pp. 1-90.
- Mitchell R.H. (2008) Petrology of hypabyssal kimberlites: relevance to primary magma compositions. *J. Volcanol. Geotherm. Res. J.* **174**, 1–8.
- Mitchell, R.H. (2020) Igneous rock associations 26. Lamproites, exotic potassic alkaline rocks: a review of their nomenclature, characterization and origins. *Geosci. Can.* **47**, 119–142.
- Moussallam Y., Morizet Y. and Gaillard F. (2016) H₂O–CO₂ solubility in low SiO₂-melts and the unique mode of kimberlite degassing and emplacement. *Earth Planet. Sci. Lett.* **447**, 151–160.
- Nakanishi N., Giuliani A., Carlson R.W., Horan M.F., Woodhead J., Pearson D.G. and Walker R.J. (2021) Tungsten-182 evidence for an ancient kimberlite source. *Proc. Natl. Acad. Sci.* **118**.
- Nie N.X., Dauphas N., Alp E.E., Zeng H., Sio C.K., Hu J.Y., Chen X., Aarons S.M., Zhang Z. and Tian H.-C. (2021) Iron, magnesium, and titanium isotopic fractionations between garnet, ilmenite, fayalite, biotite, and tourmaline: Results from NRIXS, ab initio, and study of mineral separates from the Moosilauke metapelite. *Geochim. Cosmochim. Acta* **302**, 18–45.
- Nielsen T.F. and Sand K.K. (2008) The Majuagaa kimberlite dike, Maniitsoq region, West Greenland: constraints on an Mg-rich silicocarbonatitic melt composition from groundmass mineralogy and bulk compositions. *Canad. Mineral.* **46**, 1043–1061.
- Niyazova S., Kopylova M., Gaudet M. and de Stefano A. (2022) Petrographic and geochemical characteristics associated with felsic xenolith assimilation in kimberlite. *Can. Mineral.* **60**, 283–307.

- O'Brien H. and Lehtonen M. (2012) Craton mantle formation and structure of Eastern Finland Mantle: evidence from kimberlite-derived mantle xenoliths, xenocrysts and diamonds, From the Earth's Core to Outer Space. Springer, 61–80.
- Pandey A. and Rao N.C. (2020) Supercontinent transition as a trigger for ~ 1.1 Gyr diamondiferous kimberlites and related magmatism in India. *Lithos* **370**, 105620.
- Pandey A., Rao N.C., Chakrabarti R., Pandit D., Pankaj P., Kumar A. and Sahoo S. (2017) Petrogenesis of a Mesoproterozoic shoshonitic lamprophyre dyke from the Wajrakarur kimberlite field, eastern Dharwar craton, southern India: Geochemical and Sr-Nd isotopic evidence for a modified sub-continental lithospheric mantle source. *Lithos* **292**, 218–233.
- Pearson D. and Wittig N. (2014) The formation and evolution of cratonic mantle lithosphere—evidence from mantle xenoliths, in: Carlson, R.W. (Ed.), *Treatise on Geochemistry*, pp. 255–292.
- Pearson D.G., Woodhead J. and Janney P.E. (2019) Kimberlites as geochemical probes of Earth's mantle. *Elements* **15**, 387–392.
- Peslier A.H., Woodland A.B. and Wolff J.A. (2008) Fast kimberlite ascent rates estimated from hydrogen diffusion profiles in xenolithic mantle olivines from southern Africa. *Geochim. Cosmochim. Acta* **72**, 2711–2722.
- Peters B.J., Carlson R.W., Day J.M. and Horan M.F. (2018) Hadean silicate differentiation preserved by anomalous $^{142}\text{Nd}/^{144}\text{Nd}$ ratios in the Réunion hotspot source. *Nature* **555**, 89–93.
- Rapp R.P., Irifune T., Shimizu N., Nishiyama N., Norman M.D. and Inoue T. (2008) Subduction recycling of continental sediments and the origin of geochemically enriched reservoirs in the deep mantle. *Earth Planet. Sci. Lett.* **271**, 14–23.
- Russell J.K., Porritt L.A., Lavallée Y. and Dingwell D.B. (2012) Kimberlite ascent by assimilation-fuelled buoyancy. *Nature* **481**, 352–356.
- Rzehak L.J., Kommescher S., Hoare L., Kurzweil F., Sprung P., Leitzke F.P. and Fonseca R.O. (2022) Redox-dependent Ti stable isotope fractionation on the Moon: implications for current lunar magma ocean models. *Contrib. Mineral. Petrol.* **177**, 81.
- Rzehak L. J., Kommescher S., Kurzweil F., Sprung P., Leitzke F. P. and Fonseca R. O. (2021) The redox dependence of titanium isotope fractionation in synthetic Ti-rich lunar melts. *Contrib. Mineral. Petrol.* **176**, 1–16.
- Sand K.K., Waight T.E., Pearson D.G., Nielsen T.F., Makovicky E. and Hutchison M.T. (2009) The lithospheric mantle below southern West Greenland: A geothermobarometric approach to diamond potential and mantle stratigraphy. *Lithos* **112**, 1155–1166.

- Sarkar S., Giuliani A., Dalton H., Phillips D., Ghosh S., Misev S. and Maas R. (2023) Derivation of lamproites and kimberlites from a common evolving source in the convective mantle: the case for southern African 'transitional kimberlites'. *J. Petrol.* **64**, egad043.
- Sarkar S., Giuliani A., Ghosh S. and Phillips D. (2021) Petrogenesis of coeval lamproites and kimberlites from the Wajrakarur field, Southern India: New insights from olivine compositions. *Lithos* **406**, 106524.
- Sarkar S., Giuliani A., Phillips D., Howarth G.H., Ghosh S. and Dalton H. (2022) Sublithospheric melt input in cratonic lamproites. *Geology* **50**, 1296–1300.
- Schauble E.A. (2004) Applying stable isotope fractionation theory to new systems. *Rev. Mineral. Geochem.* **55**, 65–111.
- Schmidberger S. and Francis D. (2001) Constraints on the trace element composition of the Archean mantle root beneath Somerset Island, Arctic Canada. *J. Petrol.* **42**, 1095–1117.
- Schönbächler M., Rehkämper M., Lee D.-C. and Halliday A.N. (2004) Ion exchange chromatography and high precision isotopic measurements of zirconium by MC-ICP-MS. *Analyst* **129**, 32–37.
- Shaikh A.M., Kumar S.P., Patel S.C., Thakur S.S., Ravi S. and Behera D. (2018) The P3 kimberlite and P4 lamproite, Wajrakarur kimberlite field, India: mineralogy, and major and minor element compositions of olivines as records of their phenocrystic vs xenocrystic origin. *Mineral. Petrol.* **112**, 609–624.
- Siebert C., Nägler T.F. and Kramers J.D. (2001) Determination of molybdenum isotope fractionation by double-spike multicollector inductively coupled plasma mass spectrometry. *Geochem. Geophys. Geosyst.* **2**.
- Simon N.S., Carlson R.W., Pearson D.G. and Davies G.R. (2007) The origin and evolution of the Kaapvaal cratonic lithospheric mantle. *J. Petrol.* **48**, 589–625.
- Smith C.B., Clark T.C., Barton E.S. and Bristow J.W. (1994) Emplacement ages of kimberlite occurrences in the Prieska region, southwest border of the Kaapvaal Craton, South Africa. *Chem. Geol.* **113**, 149–169.
- Soltys A., Giuliani A. and Phillips D. (2018a) Crystallisation sequence and magma evolution of the De Beers dyke (Kimberley, South Africa). *Mineral. Petrol.* **112**, 503–518.
- Soltys A., Giuliani A. and Phillips D. (2018b) A new approach to reconstructing the composition and evolution of kimberlite melts: a case study of the archetypal Bultfontein kimberlite (Kimberley, South Africa). *Lithos* **304**, 1–15.
- Soltys A., Giuliani A., Phillips D. and Kamenetsky V.S. (2020) Kimberlite metasomatism of the lithosphere and the evolution of olivine in carbonate-rich melts—evidence from the Kimberley kimberlites (South Africa). *J. Petrol.* **61**, egaa062.

- Soltys A., Giuliani A., Phillips D., Kamenetsky V.S., Maas R., Woodhead J. and Rodemann, T. (2016) In-situ assimilation of mantle minerals by kimberlitic magmas—Direct evidence from a garnet wehrlite xenolith entrained in the Bultfontein kimberlite (Kimberley, South Africa). *Lithos* **256**, 182–196.
- Sparks R. (2013) Kimberlite volcanism. *Annu Rev Earth Planet Sci.* **41**, 497–528.
- Sparks R., Baker L., Brown R., Field M., Schumacher J., Stripp G. and Walters A. (2006) Dynamical constraints on kimberlite volcanism. *J. Volcanol. Geotherm.* **155**, 18–48.
- Spencer L.M., Albert C., Williams H.M., Nebel O., Parkinson I.J., Smithies R.H., Bruno H., Fowler M., Moreira H. and Lissenberg C.J. (2024) Tracing hydrous eclogite melts in the source of sanukitoids. *Earth Planet. Sci. Lett.* **648**, 119067
- Stamm N. and Schmidt M.W. (2017) Asthenospheric kimberlites: volatile contents and bulk compositions at 7 GPa. *Earth Planet. Sci. Lett.* **474**, 309–321.
- Tappe S., Budde G., Stracke A., Wilson A. and Kleine T. (2020a) The tungsten-182 record of kimberlites above the African superplume: Exploring links to the core-mantle boundary. *Earth Planet. Sci. Lett.* **547**, 116473.
- Tappe S., Smart K., Torsvik T., Massuyeau M. and de Wit M. (2018) Geodynamics of kimberlites on a cooling Earth: clues to plate tectonic evolution and deep volatile cycles. *Earth Planet. Sci. Lett.* **484**, 1–14.
- Tappe S., Stracke A., van Acken D., Strauss H. and Luguet A. (2020b) Origins of kimberlites and carbonatites during continental collision—insights beyond decoupled Nd-Hf isotopes. *Earth-Sci. Rev.*, 103287.
- Torsvik T.H., Burke K., Steinberger B., Webb S.J. and Ashwal L.D. (2010) Diamonds sampled by plumes from the core–mantle boundary. *Nature* **466**, 352–355.
- Tovey M., Giuliani A., Phillips D., Pearson D.G., Sarkar C., Nowicki T. and Carlson J. (2021) The spatial and temporal evolution of primitive melt compositions within the Lac de Gras kimberlite field, Canada: Source evolution vs lithospheric mantle assimilation. *Lithos* **392**, 106142
- Wang W., Huang S., Huang F., Zhao X. and Wu Z. (2020) Equilibrium inter-mineral titanium isotope fractionation: Implication for high-temperature titanium isotope geochemistry. *Geochim. Cosmochim. Acta* **269**, 540–553.
- Waychunas G.A. (1987) Synchrotron radiation XANES spectroscopy of Ti in minerals; effects of Ti bonding distances, Ti valence, and site geometry on absorption edge structure. *Am. Mineral.* **72**, 89–101.
- Weiss Y., McNeill J., Pearson D.G., Nowell G.M. and Ottley C.J. (2015) Highly saline fluids from a subducting slab as the source for fluid-rich diamonds. *Nature* **524**, 339–342.

- White W.M. and Hofmann A.W. (1982) Sr and Nd isotope geochemistry of oceanic basalts and mantle evolution. *Nature* **296**, 821-825.
- Williams N.H., Fehr M.A., Parkinson I.J., Mandl M.B. and Schönbacher M. (2021) Titanium isotope fractionation in solar system materials. *Chem. Geol.* **568**, 120009.
- Woodhead J., Hergt J., Giuliani A., Maas R., Phillips D., Pearson D.G. and Nowell G. (2019) Kimberlites reveal 2.5-billion-year evolution of a deep, isolated mantle reservoir. *Nature* **573**, 578–581.
- Woodhead J., Hergt J., Phillips D. and Paton C. (2009) African kimberlites revisited: in situ Sr-isotope analysis of groundmass perovskite. *Lithos* **112**, 311–317.
- Xu J.-Y., Giuliani A., Li Q.-L., Lu K., Melgarejo J.C. and Griffin W.L. (2021) Light oxygen isotopes in mantle-derived magmas reflect assimilation of sub-continental lithospheric mantle material. *Nat. Commun.* **12**, 1–13.
- Yakovlev D., Kostrovitsky S., Fosu B. and Ashchepkov I. (2022) Diamondiferous kimberlites from recently explored Upper Muna Field (Siberian Craton): petrology, mineralogy and geochemistry insights. *Geol. Soc. Spec. Publ.* **513**, 71–102.
- Young E.D., Manning C.E., Schauble E.A., Shahar A., Macris C.A., Lazar C. and Jordan M. (2015) High-temperature equilibrium isotope fractionation of non-traditional stable isotopes: Experiments, theory, and applications. *Chem. Geol.* **395**, 176–195.
- Zhao X., Tang S., Li J., Wang H., Helz R., Marsh B., Zhu X. and Zhang H. (2020) Titanium isotopic fractionation during magmatic differentiation. *Contrib. Mineral. Petrol.* **175**, 1–16.
- Zhao X., Wang X.-J., Jia X., Evans N.J., Yi C., Chen L.-H., Hanyu T., Li J., Wan B. and Zhu X. (2024) Titanium isotopic fractionation during alkaline magma differentiation at St. Helena Island. *Contrib. Mineral. Petrol.* **179**, 6.
- Zhao J., Wang X.-J., Zhao X.-M., Liu J.-Q., Zeng G., Yi C.-X., Liu B., Li J., Zhu X.-K. and Chen L.-H. (2025) Titanium isotopes as a tracer of eclogite in the mantle sources of continental intraplate basalts. *Earth Planet. Sci. Lett.* **660**, 119366.
- Zindler A. and Hart S. (1986) Chemical geodynamics. *Annu. Rev. Earth Planet. Sci.* **14**, 493–571.
- Zurevinski S.E. and Mitchell R.H. (2011) Highly evolved hypabyssal kimberlite sills from Wemindji, Quebec, Canada: insights into the process of flow differentiation in kimberlite magmas. *Contrib. Mineral. Petrol.* **161**, 765–776.

Tables

Table 1 Overview of the studied samples.

Kimberlite field	samples	Petrographic type	Ti-bearing phases	Age (Ma)	geochemically enriched/depleted ^a
Kimberley (South Africa)	BUSK-1 ^b , Eyebrow 310, JJG-2151	Cal-Srp Mica-rich	Spl, Pvk, \pm Ilm, \pm Phl Phl, Spl, Pvk	86–87	enriched
	WESK-8, WWTS-P3 ^b	Mtc-rich, Cal-Ap-Phl-rich	Spl, Phl, Pvk, Ilm, \pm Rt	89	enriched
Premier/National (South Africa)	PRK-4	Cal-rich	Spl, Pvk	1153	enriched
Jwaneng (Botswana)	105/036/K7/11	Mtc-Cal	Spl, Rt	235	depleted
Murowa (Zimbabwe)	M1	Cal-Srp	Spl, Pvk	526	enriched
Igwisi Hills (Tanzania)	IGWK-1	Cal-Ap-Srp-rich	Spl, Pvk, Ttn	0.012	enriched
Koidu (Sierra Leone)	DZA-004 52.75m	Mica-rich	Phl, Spl, Pvk	120	enriched
Lac de Gras (Canada)	Leslie BV4, Rattler 4	Mtc-rich	Spl, Pvk, \pm Phl, \pm Rt	53	enriched
		Cal-Phl		60	
Conmtowayto (Canada)	Jericho	Mtc-Cal	Spl, Pvk, Rt, Ilm, Phl	173	depleted
Somerset (Canada)	Elwin Bay 1, 2	Srp-Cal	Spl, Pvk	97.5	depleted
Manitsoq (Greenland)	491741	Cal-Srp	Spl, Pvk, Ilm, Rt	558	depleted
Kuusamo (Finland)	KV001 ^b , KP-104 ^b	Cal-Srp-Mtc	Spl, Phl, Ilm, Pvk	747	depleted
Kaavi-Kuopio (Finland)	1.106 ^b 14.05	Cal-Srp	Spl, Phl, Pvk, \pm Ilm	623	depleted
		Mtc-Cal		585	
Upper Muna (Russia)	PSK 213/161-B ZAP-1 114/255	Srp-Cal	Phl, Spl, Pvk	363	depleted
				367	
Wajrakarur (India)	8312-B2E5, W4-8310	Srp-Cal	Spl, Pvk, Phl	1100	depleted

See Supplementary Material for references and more information.

^aBased on Hf-Nd isotope data.

^bSamples considered as evolved.

Abbreviations: Ap-apatite, Cal-calcite, Ilm-ilmenite, Mtc-monticellite, Phl-phlogopite, Pvk-perovskite, Rt-rutile, Srp-serpentine, Spl-spinel, Ttn-titanite

Table 2 Titanium isotope compositions of kimberlites measured in this study.

sample	pipe/dyke, field	country	TiO ₂ (wt%)	δ ⁴⁹ Ti (‰)	2SD (‰)	n
<i>kimberlites</i>						
BUSK-1 ^a	Benfontein, Kimberley	South Africa	2.73	+0.134	0.027	4
Eyebrow 310	De Beers - Eyebrow dyke, Kimberley	South Africa	1.27	+0.170	0.027	3
WESK-8	Wesselton, Kimberley	South Africa	1.99	+0.135	0.027	6
WWTS-P3 ^a	Wesselton Water Tunnel, Kimberley	South Africa	3.60	+0.137	0.027	3
JJG-2151	Jagersfontein, Kimberley	South Africa	1.04	+0.173	0.027	3
PRK-4	Premier, Premier/National	South Africa	2.53	+0.061	0.027	3
105/036/K7/11	DK-7, Jwaneng	Botswana	1.74	+0.051	0.027	5
M1	Murowa	Zimbabwe	0.56	+0.173	0.027	3
IGWK-1	Igwise Hills	Tanzania	1.99	+0.109	0.027	3
DZA-004 52.75m	Koidu, Koidu/Tonguma	Sierra Leone	2.17	+0.141	0.027	3
Leslie BV4	Leslie, Lac de Gras	Canada	0.48	+0.015	0.027	4
Rattler 4	Rattler, Lac de Gras	Canada	1.02	+0.044	0.027	5
Jericho	Jericho, Contwoyto	Canada	1.31	+0.007	0.027	3
Elwin Bay-1	Elwin Bay, Somerset	Canada	1.24	+0.035	0.027	3
Elwin Bay-2	Elwin Bay, Somerset	Canada	0.63	+0.040	0.027	8
491741	Majuagaa, Manitsoq	Greenland	2.86	+0.072	0.027	4
KV001 ^a	Kattaisenvaara, Kuusamo	Finland	3.23	+0.098	0.027	3
KP-104 ^a	Kalettomanpuro, Kuusamo	Finland	3.99	+0.053	0.027	7
14.05	Pipe 14, Kaatronlampi, Kaavi-Kuopio	Finland	2.60	+0.032	0.027	2
1.106 ^a	Pipe 1, Koskeniemi, Kaavi-Kuopio	Finland	1.47	+0.045	0.027	3
PSK 213/161	Poiskovaya, Upper Muna	Russia	2.25	+0.037	0.027	3
ZAP-1	Zapolnaya, Upper Muna	Russia	1.50	+0.055	0.027	2
8312-B2E5	Gollapalle E-5, Wajrakarur	India	2.44	+0.154	0.027	5
W4-8310	GollapalleW-4, Wajrakarur	India	2.27	+0.154	0.027	5
<i>Reference material</i>						
BHVO-2			2.73	+0.025	0.027	32

n: number of analyses

^aSamples considered as evolved

Concentration data derived by isotope dilution.

Figure captions

Fig. 1 Global elevation map showing the geographic locations of studied kimberlites and distribution of continental shields (modified from Giuliani and Pearson, 2019).

Fig. 2 Representative photomicrographs of studied kimberlites (plane-polarised light). (a) Abundant olivine macrocrysts in the Leslie kimberlite (Lac de Gras, Canada). (b) Peridotite- xenolith and olivine macrocrysts in the Majuagaa kimberlite (Maniitsoq, Greenland). (c) Groundmass of the Majuagaa kimberlite: subhedral-euhedral olivine and spinel, set in a fine groundmass of calcite, dolomite, and serpentine. (d) Rutile inclusions in olivine rim domains at contacts between xenocrystic cores and magmatic rims in the Wesselton kimberlite (Kimberley, South Africa). (e) Groundmass of the Koidu kimberlite (Sierra Leone), being composed of phlogopite, spinel, perovskite and carbonates. (d) Groundmass of the Gollapalle kimberlites (Wajrakarur, India), consisting of spinel, perovskite, phlogopite, carbonates and serpentine. Abbreviations are: ol-olivine, phl-phlogopite; pvk-perovskite; rt-rutile; spl-spinel. Additional photomicrographs of the differentiated samples from Kuusammo (Finland) and Kimberley (South Africa) can be found in Dalton et al. (2019) and Antonelli et al. (2023).

Fig. 3 Titanium isotope data of kimberlites analysed in this study. Open symbols depict evolved kimberlite varieties. Uncertainties are 2SD. Bulk Silicate Earth (BSE) estimate from Anguelova et al. (2024). The light grey shaded area indicates the range of komatiites and primitive basalts.

Fig. 4 Box plots of Ti isotope data of kimberlites (this study) and primitive mantle-derived rocks. Basalt and komatiite data from Deng et al. (2018a, 2019, 2023), Greber et al. (2017b), Hoare et al. (2020), Johnson et al. (2019, 2023), Klaver et al. (2024), Kommescher et al. (2023), Millet and Dauphas (2014), Millet et al. (2016) and Zhao et al. (2020, 2024). Ultrapotassic data from Anguelova et al. (2022) and this study (see Supplementary Material; Tables S2 and S4). The grey shaded area indicates the BSE estimate of Anguelova et al. (2024).

Fig. 5 Rayleigh fractionation modelling of kimberlite melt $\delta^{49}\text{Ti}$ evolution during progressive rutile crystallisation. The initial melt composition is assumed to be +0.02 ‰. Rutile-melt fractionation factor $\alpha_{\text{rutile-melt}}$ calculated for different crystallisation temperatures using the experimentally derived data from Hoare et al. (2022). The modelling implies that removal of >40% Ti is required from the melt into rutile to produce heavy Ti isotope compositions of +0.17 ‰.

Fig. 6 Primitive mantle normalised trace element concentration patterns of studied kimberlites. PM values from McDonough and Sun (1995). Trace element data and references are provided in the Supplementary Material (Table S1).

Fig. 7 Olivine rim compositions of kimberlites versus $\delta^{49}\text{Ti}$. Grey symbols depict samples characterised by a positive Ti anomaly ($\text{Ti}/\text{Ti}^* > 1$) indicative of Fe-Ti oxide accumulation. Olivine compositions from the literature (Table S3). Abbreviation SCLM: subcontinental lithospheric mantle.

Figures

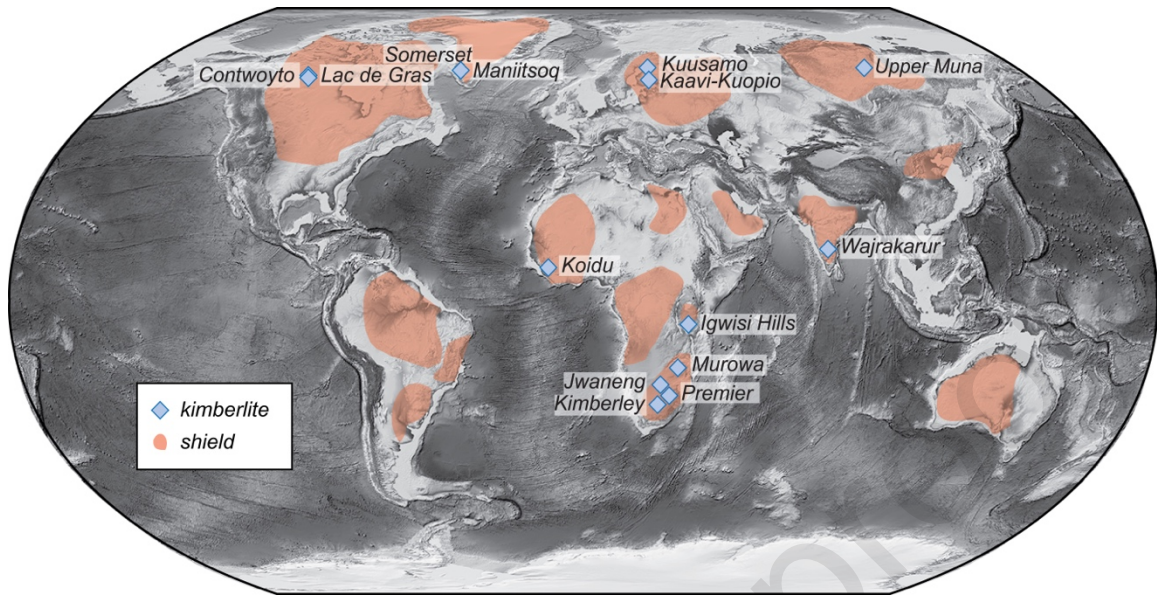


Fig. 1

Journal Pre-proof

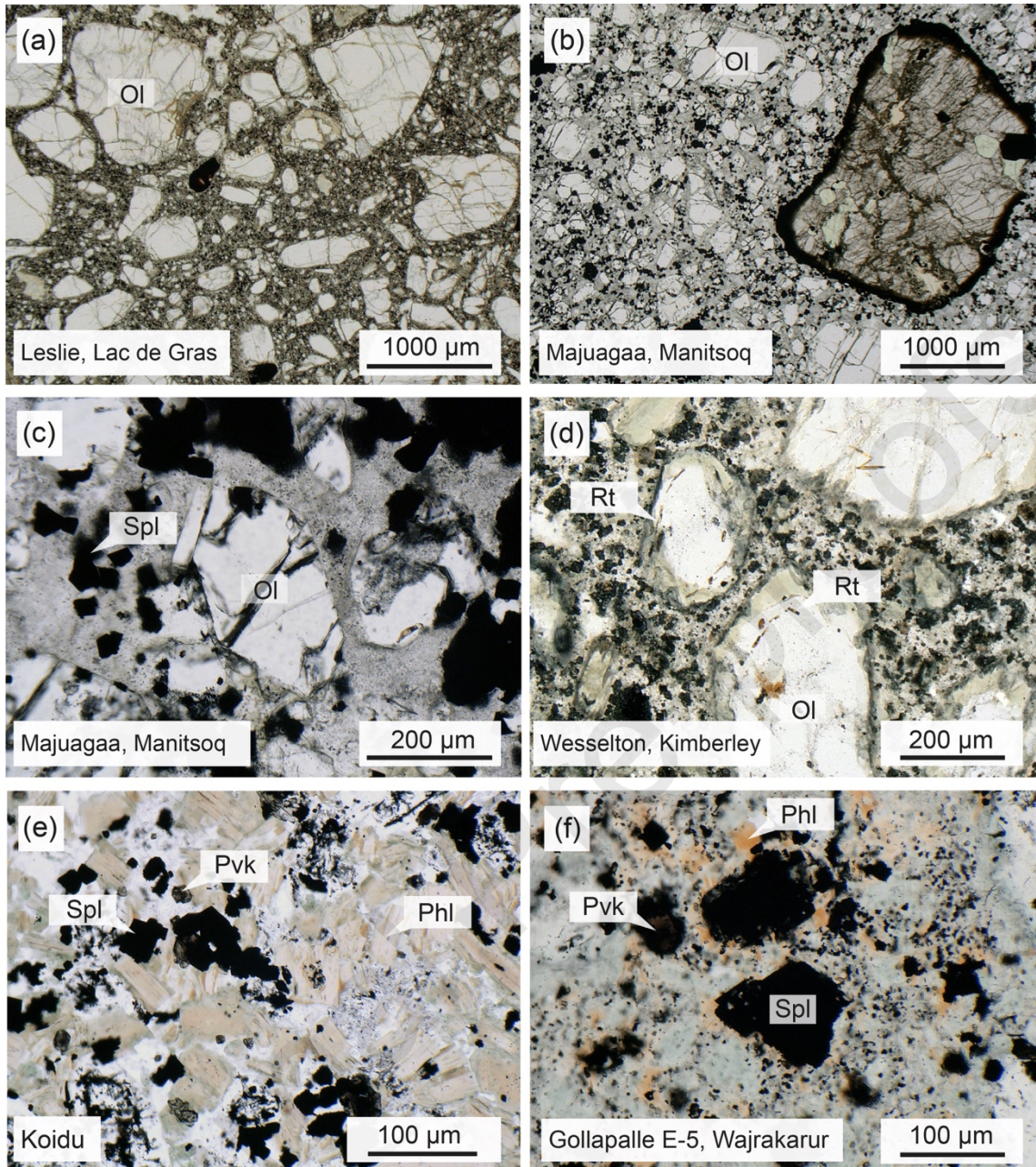


Fig. 2

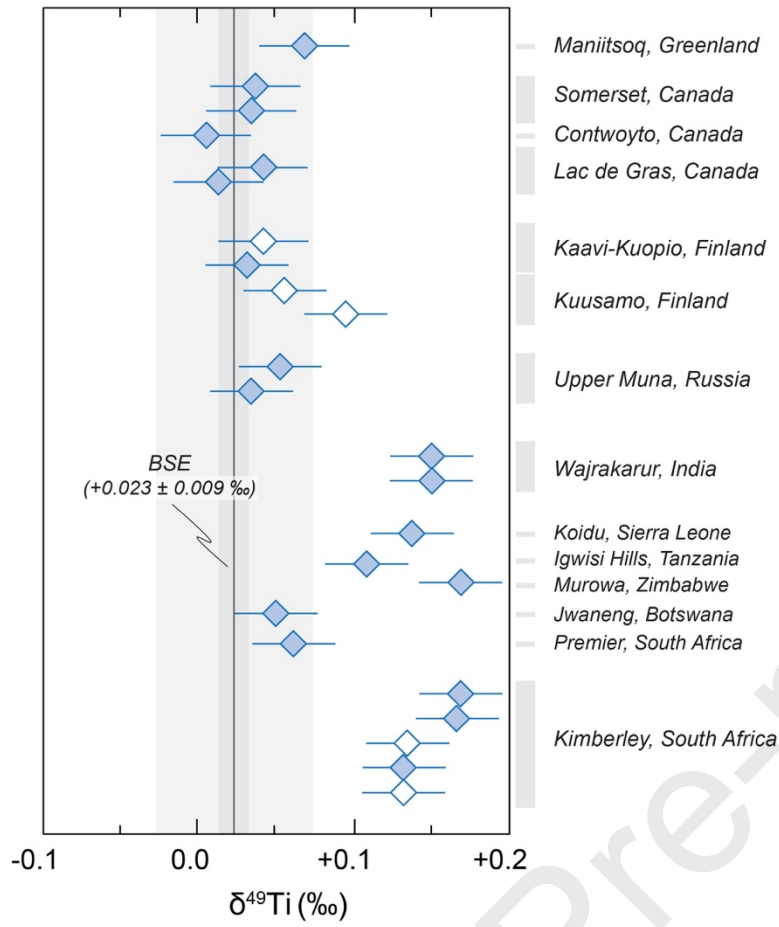


Fig. 3

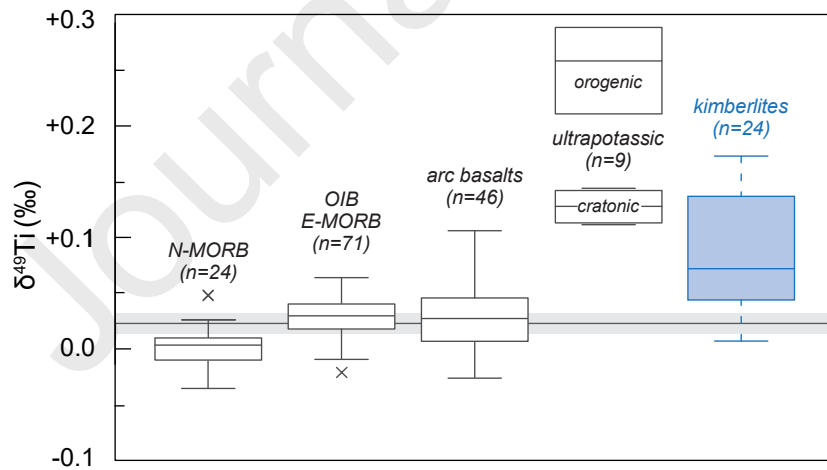


Fig. 4

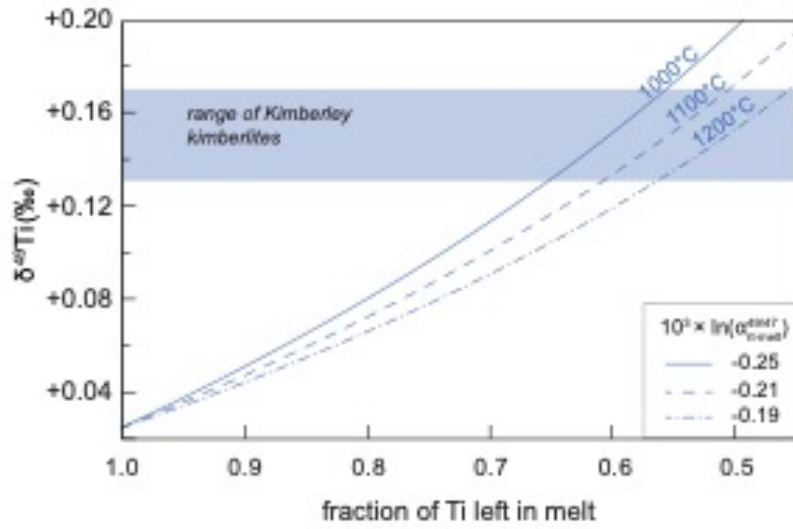


Fig. 5

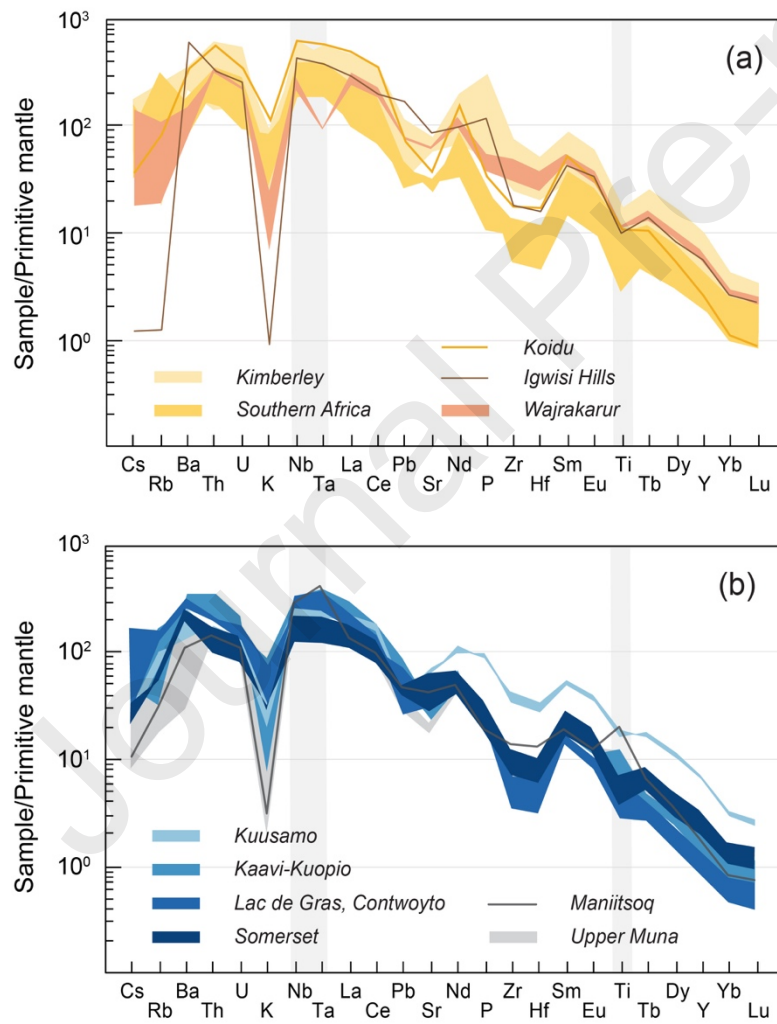


Fig. 6

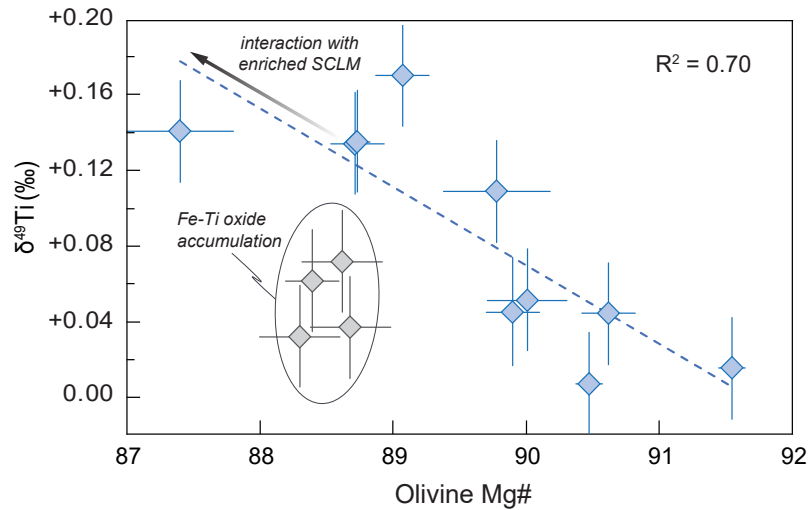


Fig. 7

Declaration of Interest Statement

The authors declare that they have no known competing financial interests or personal relationships that could have appeared to influence the work reported in this paper.

The author is an Editorial Board Member/Editor-in-Chief/Associate Editor/Guest Editor for this journal and was not involved in the editorial review or the decision to publish this article.

The authors declare the following financial interests/personal relationships which may be considered as potential competing interests: